

Data Generation using Texture Co-occurrence and Spatial Self-Similarity for Debiasing

Myeongkyun Kang¹, Dongkyu Won¹, Miguel Luna¹, Philip Chikontwe¹, Kyung Soo Hong²,
June Hong Ahn², Sang Hyun Park^{1*}

¹ Daegu Gyeongbuk Institute of Science and Technology (DGIST), Daegu, Korea

² Yeungnam University Medical Center, College of Medicine, Yeungnam University, Daegu, Korea

{mkkang, shpark13135}@dgist.ac.kr

Abstract

Classification models trained on biased datasets usually perform poorly on out-of-distribution samples since biased representations are embedded into the model. Recently, various debiasing methods have been proposed to disentangle biased representations, but it is challenging to discard only the biased features without altering other relevant information. In this paper, we propose a novel debiasing approach that explicitly generates additional images using texture representations of different labeled images to enlarge the training dataset and mitigate the bias effects when training a classifier. Every new generated image contains similar content information from a source image while transferring textures from a target image with a different label. Our model includes a texture co-occurrence loss that determines whether a generated image's texture is similar to that of the target, and a spatial self-similarity loss that determines whether the content details between the generated and source images are well preserved. Both generated and original training images are further used to train a classifier that is able to improve robustness against inconsistent bias representations. We employ five distinct artificially designed datasets with known biases to demonstrate the ability of our method to mitigate bias information. For all cases, our method outperformed existing state-of-the-art methods. Codes are available at: <https://github.com/myeongkyunkang/i2i4debias>

1. Introduction

Biases can be easily and unintentionally introduced during the data collection process. The source and properties of such biases are usually unknown, and can lead to a significant decrease in performance when a trained model uses

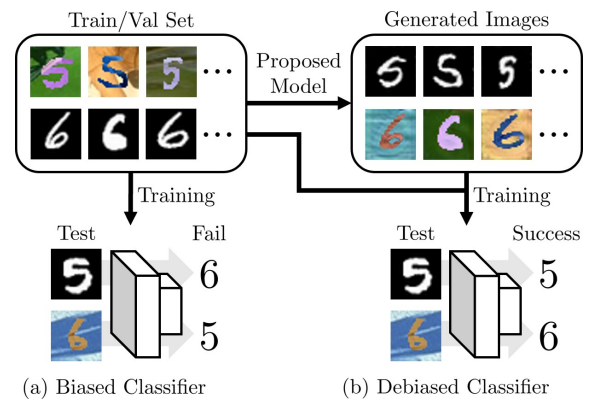


Figure 1. (a) A classifier learned using a biased dataset often gives wrong predictions. (b) We augment data by our proposed model and then use them for training a debiased classifier.

biased information to perform its intended task in out-of-distribution data [3, 4]. Therefore, it is necessary to build training data that mitigates the presence of biased characteristics such as color or texture to train reliable machine learning models. As shown in Figure 1 (a), if a binary classifier is trained with images that have a distinct texture for each class, e.g., colored digit five and grayscale six, it is highly likely that the model will consider the texture representations as a differentiator between the two classes rather than the actual numbers. In this case, the model will perform poorly on testing data that does not match the texture representations of the training data.

Bias mitigation or debiasing has been previously addressed by several methods that proposed to extract bias-independent features through adversarial learning, this enabled the model to solve the intended classification task but not bias classification (*i.e.* color) [19, 41]. However, biased representations are often retained in the models since it is difficult to completely disentangle biased features through adversarial learning. With more complex bias character-

*Corresponding author.

istics (*i.e.* real-world texture difference), bias disentanglement becomes more difficult. In addition, prior knowledge regarding the existing biases in the training data is an essential requirement for adversarial learning, but is often unknown and difficult to identify, especially when the data is collected from multiple sources [3, 4, 11, 24].

In this paper, we propose a debiasing strategy to generate new images using the existing training images by combining the content information of a source image and the texture of an image with a different label. Thus, the extended training dataset helps the classifier avoid relying on biased features to perform correct data separation. As shown in Figure 1 (b), an debiased classifier can be trained without bias labels by directly utilizing the generated images that contain the textures of images with different labels.

Modern generative adversarial networks (GAN) [14, 20, 22, 27, 32, 47] have achieved remarkable results to effectively transfer textures (or styles) between pairs of images, but they also tend to adjust content information since no supervision is provided during training. For instance, in Figure 1, one would expect the color image with five to change to a binary image with five, but a binary image containing six is mostly generated. In general, transferring texture information only without content discrepancy is very challenging, and in turn will adversely affect the classifier.

To address this issue, we propose a novel GAN that simultaneously considers spatial self-similarity between a source image and its generated image, and texture similarity between the generated image and a target image having a different label than that of the source image. The proposed GAN consists of an image generator with content and texture encoders, two discriminators that constrain texture similarity in both local and global views, and a pre-trained VGG [36] network to enforce spatial self-similarity. The generation of high quality images with the intended properties is achieved by using a *spatial self-similarity loss* to ensure content consistency, and a *texture co-occurrence loss* and *GAN loss* to enforce similar local and global textures in the target image. Once images are generated using the training data, a debiased classifier can be learned using all available data. The main contributions are listed below:

- We introduce a method to learn a debiased classifier by explicitly augmenting data rather than designing a complex model for debiasing. Our method does not require any bias labeling and can effectively mitigate unknown biases during training.
- We propose a novel image generation method employing texture co-occurrence and spatial self-similarity losses. While these losses have been respectively proposed to address different tasks, both have never been considered jointly for the image generation task. We show that optimizing both losses can produce images

that are effective for debiasing.

- We show that our method outperforms existing debiasing methods and produces high quality images compared to prior generative models on five distinct biased datasets.

2. Related Works

Debiasing and Fairness Aware Models: To mitigate bias, Alvi *et al.* [2] employed a bias prediction layer to make latent features indistinguishable using a confusion loss [38]. Kim *et al.* [19] used a gradient reversal layer [6] that minimizes the mutual information of bias predictions to constrain the use of bias-related features for classification. On the subject of fairness aware training, Li *et al.* [25] formulated bias minimization in terms of data re-sampling to balance the preference of specific representations to not be biased for classification. On the other hand, Wang *et al.* [41] employed an adversarial learning approach [6] to remove protected attributes correspondence (*e.g.* gender) in the intermediate features of the model. Moreover, Louppe *et al.* [28] proposed an adversarial network to enforce the pivotal property (*e.g.*, fairness) on a predictive model, and Zhang *et al.* [42] proposed three terms, *i.e.*, primary, adversary, and projection, to improve the stability of debias training. However, these methods require bias labels for training and stability in adversarial learning is often hard to achieve. In contrast, our method solves the bias problem by explicitly utilizing texture generated images and only requires images of different domains. Thus, our approach does not require laborious bias labeling and is free from intractable adversarial classifier training.

Image Generation and Style Transfer Models: Zhu *et al.* [47] and Liu *et al.* [27] proposed deep generative models using a pair of generators and discriminators that translate one domain into another using cycle-consistency and a shared-latent space assumption, respectively. Huang *et al.* [14] proposed a multi-domain translation model by varying the style code with a fixed content for diverse style image generation. For feature disentanglement, Lee *et al.* [22] proposed a content and attribute encoder with a cross-cycle consistency loss to enforce consistency between domains. Furthermore, Kolkin *et al.* [20] proposed an optimization-based style transfer method using the concept of self-similarity. Park *et al.* [32] proposed a conditional image translation method with a contrastive loss to maximize the mutual information between positive and negative patches, whereas Zheng *et al.* [44] proposed a spatially-correlative loss for consistent image translation to preserve scene structures. However, as most GAN-based methods focused on transferring image style from one domain to another, instead of maintaining image content; spatial discrepancy or texture corruption is observable in the generated images. Un-

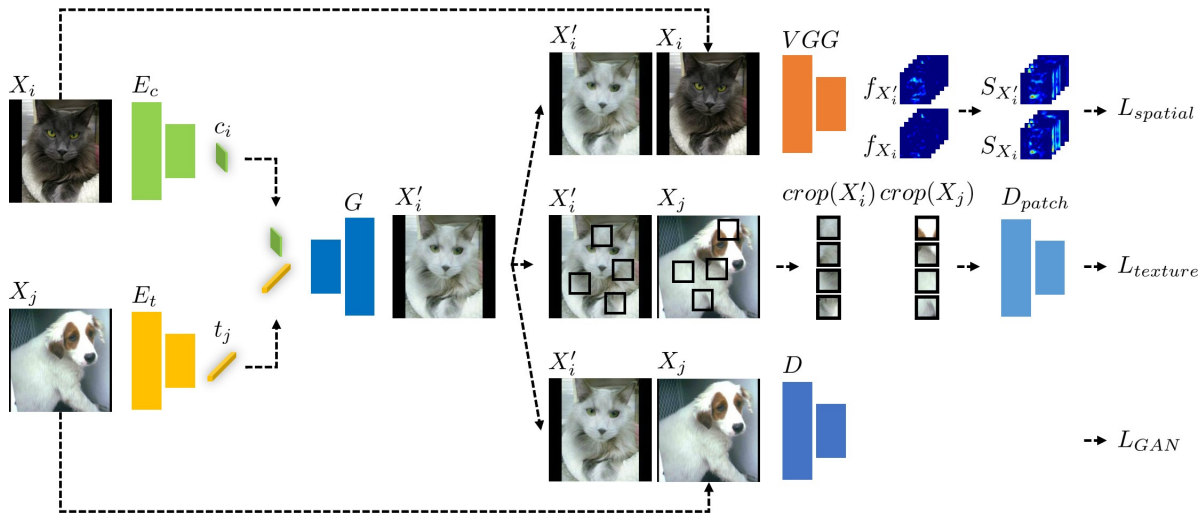


Figure 2. Our proposed image generation model. Our model consists of a content encoder E_c , texture encoder E_t , StyleGAN2 generator G , ImageNet pre-trained VGG model, and two discriminators D and D_{patch} . Each encoder extracts the content feature c_i from an image X_i and the texture feature t_j in an image X_j with a different label, respectively. G generates an image X'_i using c_i and t_j with a spatial self-similarity loss $L_{spatial}$, a texture co-occurrence loss $L_{texture}$, and a GAN loss L_{GAN} .

like prior generation models, our model only updates textures while preserving content by minimizing a spatial self-similarity loss [20].

Texture-Bias in CNN: Geirhos *et al.* [9] argued that texture bias mitigation is necessary to ensure the reliability of a classifier, since common convolutional neural networks (CNN) prioritize texture information over content (shape). Especially in the task of domain generalization [45], texture bias has gained significant interest since changes in image texture are the main reason for domain shift [23, 30, 35, 39, 40, 46]. Nuriel *et al.* [31] and Zhou *et al.* [46] applied feature-level adaptive instance normalization (AdaIN) [13] by shuffling (or swapping) the features of training samples across source domains to improve the generalizability of the trained model. Similarly, Nam *et al.* [30] introduced content- and style-biased networks that randomize the content and style (texture) features between two different samples via AdaIN. To obtain robust features to style-bias, they also leveraged adversarial learning to prevent the feature extractor from retaining style-biased representations. In general, previous methods only focus on the generalization performance of inaccessible-domain samples, and thus design models to learn common object features from multiple source domains. However, if the domain of samples are biased among the labels *e.g.*, colored digit five and grayscale digit six in Figure 1, these methods failed to learn common object features as their methods are limited to disregard the texture biases in training dataset. In this paper, we address this by training a classifier to only focus on the intended task without using bias information present in the training data.

3. Method

Given an image dataset $\mathcal{D} = \{X_1, \dots, X_n\}$ with binary classification labels $y_i \in \{0, 1\}$ and a bias property $b_i \in \{0, 1\}$ aligned with the labels *i.e.* $y_i = b_i$, our main goal is to build an augmented dataset $\mathcal{D}' = \{X'_1, \dots, X'_n\}$ that reduces the importance of b_i during the classification process. In this work, we consider texture as the dominant property that creates bias during the classification process and prevents the model from using shape information of the object of interest. Therefore, we propose a generative data augmentation framework that updates an input image X_i using the texture of a randomly selected image with a different label *i.e.*, $X_{j, y_i \neq y_j}$, while retaining the content information of X_i .

Our framework consists of three main sections as shown in Figure 2. First, X_i and X_j are encoded by a content encoder E_c and a texture encoder E_t , respectively. Then, the encoded features are used to generate a target augmented image X'_i via G , and a combination of two discriminators with an ImageNet pre-trained VGG model [36] ensure the generated image X'_i has the texture of X_j while retaining the content information of X_i . Modifying texture information while maintaining the content requires the use of additional terms in the standard adversarial objective. Thus, we add a texture co-occurrence loss term to enable correct texture transfer and a spatial self-similarity loss term to ensure the original content is unchanged. The generator G and discriminator D follow the architecture proposed in StyleGAN2 [18] and are used to compute the adversarial loss between X'_i and X_j . Texture co-occurrence loss between X_i and $X_{j, y_i \neq y_j}$ is computed by the patch-discriminator

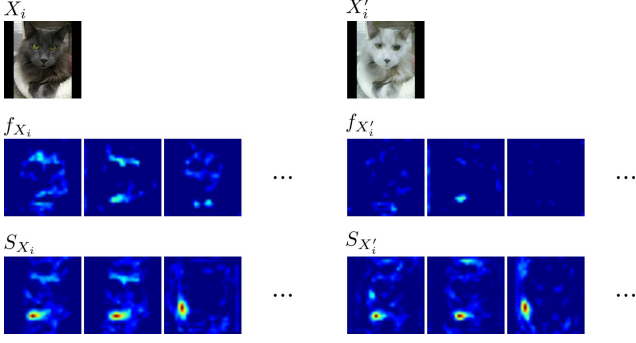


Figure 3. Visualization of intermediate feature maps obtained by *VGG* and their self-similarity maps S . Even though X_i and X'_i share the same contents, there are discrepancies between f_{X_i} and $f_{X'_i}$. On the other hand, self-similarity maps S_{X_i} and $S_{X'_i}$ are consistent.

D_{patch} , and the spatial self-similarity loss between X_i and X'_i is computed by the *VGG* model, respectively.

Finally, the original dataset \mathcal{D} is combined with its augmented version \mathcal{D}' to train a classifier that is robust to inconsistent bias representations for the classification, and can avoid bias present in the training data.

3.1. Image Generation using Content and Texture

Generating a realistic image using the content information in X_i and the texture of X_j requires the extraction of specific types of features. To this end, we use two different encoders E_c and E_t to extract a content-encoded tensor c_i and a texture-encoded vector t_j , respectively. Then, G generates a texture transferred image X'_i by taking c_i and t_j as a constant and style vector following Karras *et al.* [18], and discriminator D enforces a non-saturating adversarial loss [10] for generative training. The adversarial loss is defined as:

$$L_{GAN}(E_c, E_t, G, D) = \mathbb{E}_{X_i, X_j \sim \mathcal{D}, y_i \neq y_j} [-\log(D(G(c_i, t_j)))] \quad (1)$$

However, this setting often fails to retain content information since the discriminator is heavily enforced to generate an image that preserves entangled content features in the target domain. Thus, we add additional constraints to ensure generator G retains content information in c_i and uses texture information in t_j . These constraints take the form of two additional modules and loss terms, *i.e.*, a texture co-occurrence loss and spatial self-similarity loss.

3.2. Texture Co-occurrence Loss

To encourage the transfer of texture information t_j from X_j to X'_i *i.e.*, $G(c_i, t_j)$, we employ a texture co-occurrence loss with a patch-discriminator D_{patch} [33] that measures the texture difference between X'_i and X_j . The texture

co-occurrence loss and patch discriminator D_{patch} were initially proposed for image editing [33] to disentangle texture information from structure. D_{patch} encourages the joint feature statistics to appear perceptually similar [7, 15, 16, 33]. This is achieved by cropping multiple random patch sizes between 1/8 to 1/4 of the full image size and feeding them into D_{patch} . In particular, we average the features in X_j patches and concatenate with the features of X'_i , and feed them to the last layers of D_{patch} to calculate the discriminator loss. Consequently, G is enforced to satisfy the joint statistics of low-level features for consistent texture transfer. Formally,

$$L_{texture}(E_c, E_t, G, D_{patch}) = \mathbb{E}_{X_i, X_j \sim \mathcal{D}, y_i \neq y_j} [-\log(D_{patch}(crop(X'_i), crop(X_j)))]. \quad (2)$$

3.3. Spatial Self-Similarity Loss

To retain the content information of the source image, we employ spatial self-similarity as a domain invariant content constraint. The self-similarity loss has been used to maintain structure of content images in artistic image style transfer [20]. Formally, a spatial self-similarity map is considered as follows:

$$S_{X_i} = f_{X_i}^T \cdot f_{X_i}, \quad (3)$$

where $f_{X_i} \in \mathbb{R}^{C \times HW}$ denotes the spatially flattened features extracted from *VGG* with channel C , height H , and width W , respectively. By applying the dot product, $S_{X_i} \in \mathbb{R}^{HW \times HW}$ captures spatial correlation from one location (\mathbb{R}^C) to the rest in all feature maps. Thus, our domain invariant content constraint (spatial self-similarity loss) can be calculated between X'_i and X_i as follows:

$$L_{spatial}(E_c, E_t, G) = \mathbb{E}_{X_i, X_j \sim \mathcal{D}, y_i \neq y_j} [\|1 - \cos(S_{X_i}, S_{X'_i})\|_1], \quad (4)$$

where \cos denotes the cosine similarity. In conventional generative models, the reconstruction loss (*e.g.*, L1, MSE) or perceptual losses are used to provide constraints using the entangled feature (contents and texture) for minimizing content discrepancy (Figure 3). Since the content information can be decoupled from texture information using spatial self similarity, we can explicitly control the content features in G . Consequently, we can successfully preserve the content of X_i while updating texture.

3.4. Full Objective and Implementation Details

The objective function of our framework is defined as:

$$L_{total} = \lambda_g L_{GAN} + \lambda_t L_{texture} + \lambda_s L_{spatial}, \quad (5)$$

where hyper-parameters λ_g , λ_t , and λ_s balance the importance of spatial and texture loss terms, respectively. We set

$\lambda_g = 0.1$, $\lambda_t = 1.0$, and $\lambda_s = 100$, respectively. The objective and network design of discriminators D and D_{patch} closely follow StyleGAN2 [18]. E_c and E_t downsample their inputs 2x and 6x each to extract c_i and t_j (1x and 4x for small resolution inputs e.g. digit), respectively. For t_j , we explicitly discard spatial information by applying global average pooling. To reduce computational costs, we select 256 random features from $f_{X_i}^T$ to obtain $\hat{f}_{X_i}^T$, thus reducing the size of the self-similarity map, i.e., $\hat{S}_{X_i} = \hat{f}_{X_i}^T \cdot f_{X_i}$. Herein, $\hat{S}_{X_i} \in \mathbb{R}^{256 \times HW}$ is used to calculate $L_{spatial}$ instead of $S_{X_i} \in \mathbb{R}^{HW \times HW}$ (generally $256 < HW$). To construct \mathcal{D}' , we randomly select texture sources from images with a different label.

3.5. Extension to Multi-domain Debiasing

To debias a multi-domain biased dataset, the number of models required for texture updates is a factorial of the number of domains in the set. In other words, it is challenging to use the proposed method on datasets with a large number of labels (domains). Herein, we introduce a conditional version of the proposed method that can be constructed by using 2D embedding layers that simply changing the statistics of an intermediate feature \mathcal{F} of CNN. The domain label is fed into a 2D embedding layer and returns 1D vectors (weight e_w and bias e_b in the same dimensions as \mathcal{F}) used for feature updates i.e., $\mathcal{F}' = \mathcal{F} \times e_w + e_b$. The updated feature \mathcal{F}' is fed to the next layer instead of \mathcal{F} . Consequently, a condition is provided to the model. We feed the 2D embedding layers to the second and pre-last CNN layers of E_c , E_t , and D . For c_i , t_j , and the cropped patches fed G and D_{patch} , no condition is employed.

4. Experiments

4.1. Datasets

Existing datasets often have similar distributions between training and testing data [3, 4], making them unsuitable for direct bias mitigation analysis. Thus, we constructed five biased datasets between training and testing following previous works [2, 19] to correctly evaluate bias mitigation. Visual examples are shown in Figure 4.

Five vs. Six: This set is based on MNIST [21] and MNIST-M [6] datasets where only the numbers five and six are used to construct a training split. Images with a five are taken solely from MNIST-M, whereas those with six are from MNIST, the opposite case is considered for the testing split.

Dogs vs. Cats: This dataset was originally proposed by Kim *et al.* [19] by aligning the hair color differences of animals. Bright dog and dark cat images are taken for a training split. On the other hand, dark dog and bright cat images are taken for a testing split. Consequently, the dataset is biased towards hair color.

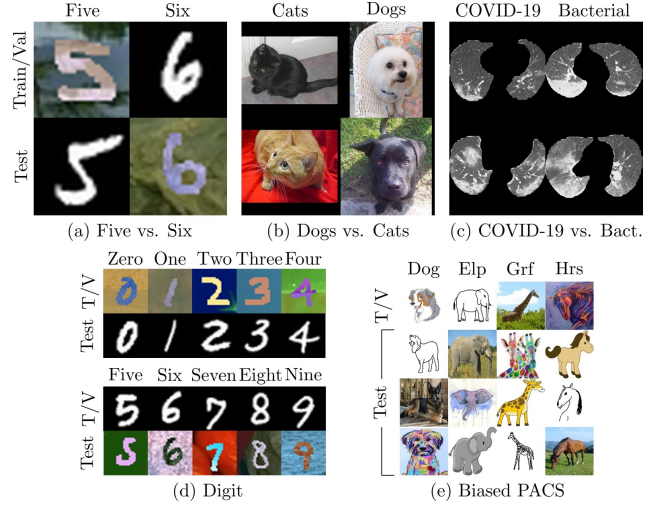


Figure 4. Examples of biased datasets. T/V indicates Train/Val. Elp, Grf, and Hrs in Biased PACS (e) indicate elephant, giraffe, and horse. (best viewed while zoomed in)

COVID-19 vs. Bacterial pneumonia: Pneumonia caused by different pathogens requires specific treatments. However, images obtained by computed tomography (CT) scans might share similar properties making accurate diagnosis challenging. One source of ambiguity for automatic diagnostic systems is the choice of a CT protocol during the image acquisition process, i.e., using a Contrast agent vs. another protocol. To evaluate our method on the real-world bias, the CT scans were collected at anonymous medical center. In this dataset, we selected Non-contrast COVID-19 for training and contrasted scans for testing. The opposite applies for Bacterial pneumonia scans.

Multi-class Biased Datasets: To evaluate our method on a multi-class biased dataset, we constructed **Digit** and **Biased PACS** datasets. In the Digit dataset, samples with labels from zero to four are taken from MNIST [21], and those from five to nine from MNIST-M [6]. Biased PACS dataset was constructed using PACS dataset [23], which consists of four domains (Photo, Art, Cartoon, Sketch) and has seven classes. We selected the top four labels (Dog, Elephant, Giraffe, Horse) after sorting the number of images. Each class is taken from a different domain (e.g., Dog - Cartoon, Elephant - Sketch) for the training dataset, and the remaining domain images are used for the test set. Additionally, we constructed an **Inverse Biased PACS** dataset that inversely uses the biased PACS dataset, i.e., replace the test split samples with the training samples, and replace the train/val split samples with the testing samples, respectively. Compared to the binary-class biased datasets, this dataset has access to samples in three domains during training and be evaluated on samples from a single domain that does not match the training data.

Table 1. Classification performances of non-generative debiasing methods (The first sub-row), domain generalization methods (The second sub-row), image generative models (The third sub-row), and the proposed model (The fourth sub-row) on five datasets. F1-score with \pm std was used for the measurement. The second and third sub-column indicate binary- and multi-class biased dataset classification performances, respectively.

Method	(a) Five vs. Six	(b) Dogs vs. Cats	(c) COV. vs. Bact.	(d) Digit	(e) B. PACS	(e') Inv. B. PACS
Baseline [12]	1.81 \pm 0.04	67.27 \pm 2.21	48.63 \pm 9.81	3.96 \pm 1.47	12.89 \pm 2.84	29.01 \pm 2.04
Learn to Pivot [28]	1.42 \pm 0.52	73.85 \pm 2.20	66.53 \pm 7.59	-	-	-
Adv. Debias [42]	1.27 \pm 0.21	72.42 \pm 3.01	59.71 \pm 6.57	-	-	-
BlindEye [2]	1.60 \pm 0.76	77.13 \pm 4.72	65.75 \pm 4.07	3.93 \pm 1.26	10.72 \pm 1.34	28.33 \pm 3.24
Not Enough [41]	1.82 \pm 1.02	72.06 \pm 3.49	61.57 \pm 5.24	6.20 \pm 3.23	10.23 \pm 1.31	37.58 \pm 12.45
LNLT [19]	2.85 \pm 1.91	69.35 \pm 5.78	61.57 \pm 5.24	11.26 \pm 1.91	12.16 \pm 2.46	34.04 \pm 5.76
P-AdaIN [31]	1.67 \pm 0.70	73.21 \pm 4.60	59.71 \pm 6.57	1.85 \pm 0.61	11.83 \pm 1.06	37.46 \pm 5.89
MixStyle [46]	16.47 \pm 9.36	72.51 \pm 3.08	55.78 \pm 7.96	5.54 \pm 3.28	10.39 \pm 0.96	34.80 \pm 1.44
CycleGAN [47]	23.07 \pm 2.47	89.66 \pm 1.20	59.33 \pm 2.42	1.90 \pm 0.21	-	-
UNIT [27]	1.09 \pm 0.65	85.80 \pm 3.10	59.96 \pm 10.04	6.30 \pm 0.84	-	-
MUNIT [14]	1.48 \pm 0.33	86.81 \pm 1.81	65.54 \pm 7.93	8.61 \pm 1.05	-	-
DRIT++ [22]	31.85 \pm 2.34	80.87 \pm 1.61	47.07 \pm 9.91	30.80 \pm 0.93	-	-
CUT [32]	6.50 \pm 0.78	86.19 \pm 1.22	52.75 \pm 15.45	2.96 \pm 0.72	-	-
Proposed	75.18 \pm 3.52	91.80 \pm 0.44	76.50 \pm 3.38	68.82 \pm 1.27	-	-
Proposed (Ext.)	72.62 \pm 2.56	90.80 \pm 0.59	70.70 \pm 5.80	63.82 \pm 0.71	36.68 \pm 1.24	46.48 \pm 4.09

4.2. Experimental Settings

For our baseline, we train an ImageNet pre-trained ResNet50 classifier only using the biased training data without any debiasing methods. For COVID-19 vs. Bacterial pneumonia, we aggregated slice predictions via majority voting to obtain patient-level diagnosis. We evaluated accuracy using the macro F1-score, which treats the label distribution equally. For consistency, training was repeated three times, and we report the averaged performance with the standard deviation of each method as the final performance.

We compare our method against five conventional debiasing methods [2, 19, 28, 41, 42], two domain generalization methods [31, 46], and five generative models [14, 22, 27, 32, 47]. For non-generative debiasing methods, bias information (e.g., data-source, color, and CT protocol) was used to train the classifier. For generative models, we constructed augmented datasets using each generative model and employed them to train classifiers. For fair evaluation, the classifiers in the compared methods were trained using the same backbone (ResNet50) using the same training settings. In the multi-domain data experiments, we did not perform the experiments of the methods [28, 42] proposed as a binary classification method and the generation methods [14, 22, 27, 32, 47] that had to learn models between all domain labels.

5. Results

Five vs. Six: In this task, none of the compared models yielded satisfactory results (see Table 1 (a)). Non-generative models report extremely low scores, implying that texture was used as the main feature for classification

instead of the digit. Furthermore, domain generalization methods also show poor F1-scores. On the other hand, we observed that generative models mainly transferred texture and shape jointly (See Figure 5). Consequently, the resulting augmented dataset had several instances with the shape of a different label. As the classifier does not have a clear cue to distinguish between numbers, this led to poor performance. This dataset clearly shows the benefit of using our method to transfer texture features while retaining the underlying information for successful bias mitigation.

Dogs vs. Cats: Performing classification on real-world animals requires more complex features than color alone. In Table 1. (b), we observed an increase in performance when a debiasing- or domain generalization method was applied. Overall, generative models show better performance over the non-generative counterparts, *i.e.* F1-score +10%. While the performance of generative models was reasonable, several limitations were noted. In the case of CycleGAN, CUT, and DRIT++, unsatisfactory images were obtained, *i.e.*, texture was not entirely translated and distortions were present. Moreover, UNIT and MUNIT generate images with small texture updates, thus bias remains in the generated images (see Figure 5). On the other hand, our model simultaneously shows improved performance with high-quality image generation. We believe this is mainly due to the proposed texture translation strategy. Leveraging both texture co-occurrence and spatial self-similarity losses enabled our model to generate consistent and natural images leading to improved classification performance.

COVID-19 vs. Bacterial Pneumonia: In contrast to the results observed on the Dogs vs. Cats task, non-generative models report improved performance over the rest (Table 1. (c)). Domain generalization methods obtain lower

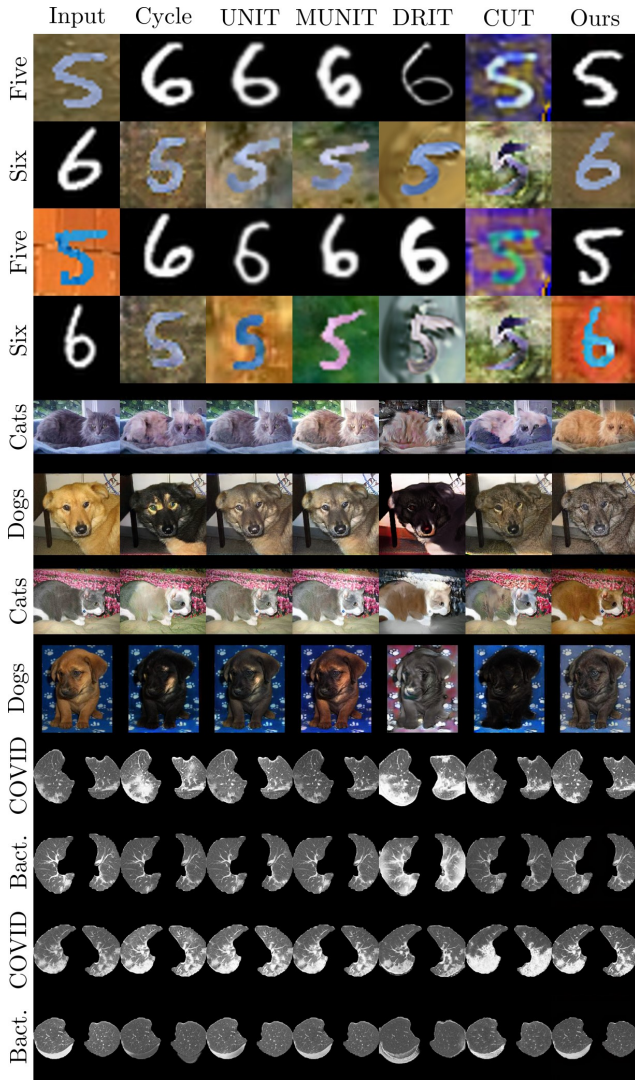


Figure 5. Qualitative results on five generative models and ours. Our model uses the content from the source image and the texture from the different label image. For each dataset, same row image is used as source and the texture is coming from the opposite pair. Our model successfully transfers texture while retaining the content. (best viewed zoomed in)

F1-scores than non-generative approaches, whereas non-generative models mitigate distinctly recognizable bias in the image such as color than generative models since they do not impose any structural changes on images. On the other hand, generative-based models tend to modify patterns on regions of diagnostic interest, thus losing the properties that identify the disease and leading to lower performance (See Figure 5). For example, CycleGAN tends to erase (row 10, 12) or create lesions (row 9) in the CT scans. UNIT and MUNIT show minor texture updates, hence are insufficient to mitigate the bias by the classifier

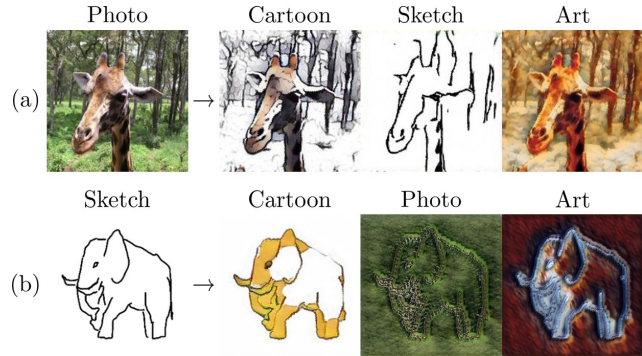


Figure 6. Qualitative results of the proposed method on the Biased PACS dataset. (a) Cartoon, sketch, and art images are generated from a photo image. (b) Cartoon, photo, and art images are generated from a sketch image.

during training (all rows). DRIT++ and CUT create artifacts such as non-existent lesions, checkerboards and change the images’ properties (row 9, 10, 12), resulting in the lowest classification accuracy among the generative models. Meanwhile, our method jointly optimizes the texture co-occurrence and spatial self-similarity losses, each imposing structural and texture constraints for image generation. Herein, our method can successfully update texture without introducing artifacts in the original CT scan.

Multi-class Biased Datasets: For the multi-class Digit dataset, none of non-generative models and domain generalization methods report satisfactory performance (see Table 1. (d)). On the other hand, our method achieved the best score over all compared methods (*i.e.* 68.82%). For the Biased PACS dataset, all comparison methods report F1-scores around 10%, while our method significantly improved to 36.68% (Table 1. (e)). The translated images from Photo to other domains are compromised as shown in Figure 6. (a), whereas Sketch to Photo (and Art) have differences between the realistic Photo (and Art) images as shown in Figure 6. (b). We found that this is due to the scale of Biased PACS dataset (small with only a few hundred images). Despite this, our method achieves reasonable generation quality, retains content and accurately transfers textures for debiasing. For Inverse Biased PACS dataset, even though non-generative models and domain generalization methods utilize multiple domain samples for training, they perform poorly on out-of-distribution samples as shown Table 1 (e’). This implies a difficulty in learning domain agnostic features. In summary, we empirically show that images generated with our method can help the classifier mitigate biases towards improved performance and can be applied to not only binary-domain & binary-class classification, but also multi-domain & multi-class classification tasks.

Ablation Study: We performed ablation studies to evalu-

Table 2. Classification performances of the ablation study of the proposed model using F1-score with \pm std on three datasets. w/o L_s and w/o L_t indicate training without $L_{spatial}$ and $L_{texture}$, respectively. Replace L_s , Replace L_t , and Replace L_s & L_t indicate replacing with perceptual loss [8], style loss [26], and perceptual & style loss for each loss function.

Method	Five vs. Six	Dogs vs. Cats	COV. vs. Bact.
w/o L_s	63.88 ± 4.97	69.92 ± 6.50	52.68 ± 4.80
w/o L_t	3.57 ± 1.93	88.28 ± 0.98	48.19 ± 5.92
Re. L_s	56.87 ± 1.26	89.45 ± 0.92	52.68 ± 16.04
Re. L_t	13.16 ± 1.64	87.07 ± 1.61	42.47 ± 5.21
Re. L_s & L_t	19.08 ± 10.37	86.95 ± 0.93	48.59 ± 5.58
Proposed	75.18 ± 3.52	91.80 ± 0.44	76.50 ± 3.38

ate the impact of the content $L_{spatial}$ and texture $L_{texture}$ losses by either removing one or replacing them with a different loss function. It is essential to validate whether texture co-occurrence and self-similarity are the key components for improving image generation quality in biased settings. Thus, we used style [26] and perceptual [8] losses to replace $L_{spatial}$ and $L_{texture}$, respectively, as they are the most common techniques widely used in style transfer to retain content features in image generation. Results on the Five vs. Six dataset in Table 2 show that the use of texture co-occurrence is a vital component to enable the classifier to correctly differentiate digits. However, qualitative results in Figure 7 indicate that the absence of $L_{texture}$ results in a failure to change the texture and correctly mitigate the bias information. Likewise, replacing $L_{texture}$ with style loss overcomes the content constraints by modifying both texture and shape. In addition, while the absence of $L_{spatial}$ lets the classifier achieve higher performance than most methods, qualitative results show that even though the texture is correct, the shape does not resemble neither a number five nor six, which can be exploited by the binary classifier and can lead to incorrect prediction. Moreover, replacing $L_{spatial}$ or $L_{spatial}$ & $L_{texture}$ results in poor image quality with ambiguous shapes. Consequently, we show that the combination of texture co-occurrence and self-similarity losses leads to higher image quality towards mitigating the underlying bias.

For Dogs vs. Cats, the model seems to be less susceptible to a drop in performance due to a change in the loss term, and usually generates good quality images as is reflected by the good classification results. The only exception is the absence of $L_{spatial}$, which reported a lower score (Table 2), and it is clear from Figure 7 that the shape is lost in a similar fashion to the results observed in Five vs. Six data. In contrast, COVID-19 vs. Bacterial pneumonia results show high dependency on the loss functions leading to decrease in performance across all ablation studies. We believe this due to the explicit criteria of content and texture are important to reduce the risk of unintended dis-

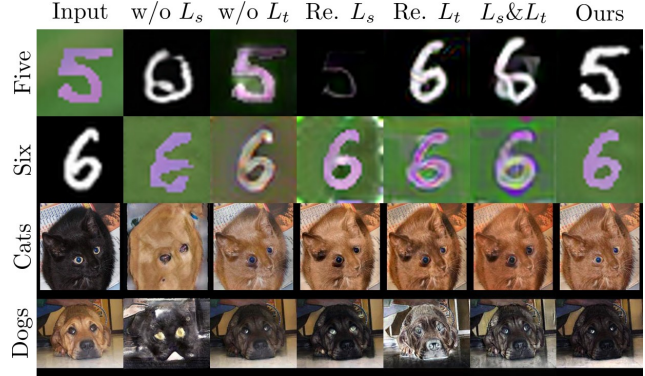


Figure 7. Qualitative results on ablation studies. L_s and L_t indicates $L_{spatial}$ and $L_{texture}$. Re. L_s , Re. L_t , and L_s & L_t indicate replacing with perceptual loss, style loss, and perceptual & style loss for each loss function. (best viewed zoomed in)

tortion and insufficient texture translation, respectively. In summary, the ablation studies show that our loss function design choices played an essential role in alleviating the inherited bias problem observed in training data, and proved that our method could mitigate bias across multiple datasets with high performance by adopting an image generation strategy.

6. Limitations

In this paper, we analyzed the relationship between image generation and debiasing performance, and showed that our method achieves significant performance improvements over prior methods on several biased datasets. However, experiments were performed on small-scale datasets with limited domains and classes. For large-scale multi-domain and multi-class training, we believe training would be difficult. Thus, an additional module and training strategy would be required to ensure convergence in model training. Additionally, we believe constructing such a large-scale multi-class dataset to evaluate bias mitigation is non-trivial. Therefore, we leave these tasks for our future research.

7. Conclusion

In this work, we have proposed a novel strategy to augment an initially biased dataset with new instances that mitigate the biased properties using a generative model. We have demonstrated that a dataset extended by our proposed method can be used to train a debiased classifier, and the strategy of transferring texture while maintaining content information is a valid choice for addressing data bias in multiple types of datasets. In particular, our model was able to handle simple biases such as color and texture, as well as more complex and realistic features like those induced by different CT scanning protocols. Our results show that

using both texture co-occurrence and spatial self-similarity losses to impose constraints in our generative model is key, as the losses are complementary. Finally, we report high accuracy with large margins across all evaluated datasets and generated higher quality images compared to prior state-of-the-art methods.

References

- [1] Hugo JWL Aerts, Emmanuel Rios Velazquez, Ralph TH Leijenaar, Chintan Parmar, Patrick Grossmann, Sara Carvalho, Johan Bussink, René Monshouwer, Benjamin Haibe-Kains, Derek Rietveld, et al. Decoding tumour phenotype by noninvasive imaging using a quantitative radiomics approach. *Nature communications*, 5(1):1–9, 2014. **15**
- [2] Mohsan Alvi, Andrew Zisserman, and Christoffer Nellåker. Turning a blind eye: Explicit removal of biases and variation from deep neural network embeddings. In *Proceedings of the European Conference on Computer Vision Workshops*, 2018. **2, 5, 6, 16**
- [3] Andrei Barbu, David Mayo, Julian Alverio, William Luo, Christopher Wang, Dan Gutfreund, Josh Tenenbaum, and Boris Katz. Objectnet: A large-scale bias-controlled dataset for pushing the limits of object recognition models. In *Advances in Neural Information Processing Systems*, volume 32, 2019. **1, 2, 5**
- [4] Alceu Bissoto, Eduardo Valle, and Sandra Avila. Debiasing skin lesion datasets and models? not so fast. In *Proceedings of the IEEE/CVF Conference on Computer Vision and Pattern Recognition Workshops*, pages 740–741, 2020. **1, 2, 5**
- [5] Jifeng Dai, Haozhi Qi, Yuwen Xiong, Yi Li, Guodong Zhang, Han Hu, and Yichen Wei. Deformable convolutional networks. In *Proceedings of the IEEE international conference on computer vision*, pages 764–773, 2017. **15**
- [6] Yaroslav Ganin and Victor Lempitsky. Unsupervised domain adaptation by backpropagation. In *Proceedings of the 32nd International Conference on Machine Learning*, volume 37, pages 1180–1189, 2015. **2, 5**
- [7] Leon Gatys, Alexander S Ecker, and Matthias Bethge. Texture synthesis using convolutional neural networks. *Advances in neural information processing systems*, 28:262–270, 2015. **4**
- [8] Leon A Gatys, Alexander S Ecker, and Matthias Bethge. Image style transfer using convolutional neural networks. In *Proceedings of the IEEE conference on computer vision and pattern recognition*, pages 2414–2423, 2016. **8**
- [9] Robert Geirhos, Patricia Rubisch, Claudio Michaelis, Matthias Bethge, Felix A Wichmann, and Wieland Brendel. Imagenet-trained cnns are biased towards texture; increasing shape bias improves accuracy and robustness. In *International Conference on Learning Representations*, 2019. **3**
- [10] Ian Goodfellow, Jean Pouget-Abadie, Mehdi Mirza, Bing Xu, David Warde-Farley, Sherjil Ozair, Aaron Courville, and Yoshua Bengio. Generative adversarial nets. *Advances in neural information processing systems*, 27, 2014. **4**
- [11] Yash Goyal, Tejas Khot, Douglas Summers-Stay, Dhruv Batra, and Devi Parikh. Making the v in vqa matter: Elevating the role of image understanding in visual question answering. In *Proceedings of the IEEE Conference on Computer Vision and Pattern Recognition (CVPR)*, July 2017. **2**
- [12] Kaiming He, Xiangyu Zhang, Shaoqing Ren, and Jian Sun. Deep residual learning for image recognition. In *Proceedings of the IEEE conference on computer vision and pattern recognition*, pages 770–778, 2016. **6, 16**
- [13] Xun Huang and Serge Belongie. Arbitrary style transfer in real-time with adaptive instance normalization. In *Proceedings of the IEEE International Conference on Computer Vision*, pages 1501–1510, 2017. **3**
- [14] Xun Huang, Ming-Yu Liu, Serge Belongie, and Jan Kautz. Multimodal unsupervised image-to-image translation. In *Proceedings of the European Conference on Computer Vision (ECCV)*, 2018. **2, 6, 11, 16**
- [15] Bela Julesz. Visual pattern discrimination. *IRE transactions on Information Theory*, 8(2):84–92, 1962. **4**
- [16] Bela Julesz. Textons, the elements of texture perception, and their interactions. *Nature*, 290(5802):91–97, 1981. **4**
- [17] Ma Jun, G Cheng, W Yixin, A Xingle, G Jiantao, Y Ziqi, Z Mingqing, L Xin, D Xueyuan, C Shucheng, et al. Covid-19 ct lung and infection segmentation dataset. *Zenodo*, Apr, 20, 2020. **15**
- [18] Tero Karras, Samuli Laine, Miika Aittala, Janne Hellsten, Jaakko Lehtinen, and Timo Aila. Analyzing and improving the image quality of stylegan. In *Proceedings of the IEEE/CVF Conference on Computer Vision and Pattern Recognition*, pages 8110–8119, 2020. **3, 4, 5**
- [19] Byungju Kim, Hyunwoo Kim, Kyungsu Kim, Sungjin Kim, and Junmo Kim. Learning not to learn: Training deep neural networks with biased data. In *Proceedings of the IEEE/CVF Conference on Computer Vision and Pattern Recognition*, pages 9012–9020, 2019. **1, 2, 5, 6, 16**
- [20] Nicholas Kolkin, Jason Salavon, and Gregory Shakhnarovich. Style transfer by relaxed optimal transport and self-similarity. In *Proceedings of the IEEE/CVF Conference on Computer Vision and Pattern Recognition (CVPR)*, June 2019. **2, 3, 4**
- [21] Yann LeCun, Corinna Cortes, and CJ Burges. Mnist handwritten digit database. *ATT Labs [Online]*. Available: <http://yann.lecun.com/exdb/mnist>, 2, 2010. **5**
- [22] Hsin-Ying Lee, Hung-Yu Tseng, Qi Mao, Jia-Bin Huang, Yu-Ding Lu, Maneesh Kumar Singh, and Ming-Hsuan Yang. Dri++: Diverse image-to-image translation via disentangled representations. *International Journal of Computer Vision*, pages 1–16, 2020. **2, 6, 11, 16**
- [23] Da Li, Yongxin Yang, Yi-Zhe Song, and Timothy M Hospedales. Deeper, broader and artier domain generalization. In *Proceedings of the IEEE international conference on computer vision*, pages 5542–5550, 2017. **3, 5**
- [24] Yingwei Li, Yi Li, and Nuno Vasconcelos. Resound: Towards action recognition without representation bias. In *Proceedings of the European Conference on Computer Vision (ECCV)*, September 2018. **2**
- [25] Yi Li and Nuno Vasconcelos. Repair: Removing representation bias by dataset resampling. In *Proceedings of the IEEE/CVF Conference on Computer Vision and Pattern Recognition (CVPR)*, June 2019. **2**

- [26] Yanghao Li, Naiyan Wang, Jiaying Liu, and Xiaodi Hou. Demystifying neural style transfer. In *Proceedings of the 26th International Joint Conference on Artificial Intelligence, IJ-CAI'17*, page 2230–2236, 2017. 8
- [27] Ming-Yu Liu, Thomas Breuel, and Jan Kautz. Unsupervised image-to-image translation networks. In I. Guyon, U. V. Luxburg, S. Bengio, H. Wallach, R. Fergus, S. Vishwanathan, and R. Garnett, editors, *Advances in Neural Information Processing Systems*, volume 30, 2017. 2, 6, 11, 16
- [28] Gilles Louppe, Michael Kagan, and Kyle Cranmer. Learning to pivot with adversarial networks. In I. Guyon, U. V. Luxburg, S. Bengio, H. Wallach, R. Fergus, S. Vishwanathan, and R. Garnett, editors, *Advances in Neural Information Processing Systems*, volume 30, 2017. 2, 6, 16
- [29] SP Morozov, AE Andreychenko, NA Pavlov, AV Vladzmyrskyy, NV Ledikhova, VA Gombolevskiy, Ivan A Blokhin, PB Gelezhe, AV Gonchar, and V Yu Chernina. Mosmeddata: Chest ct scans with covid-19 related findings dataset. *arXiv preprint arXiv:2005.06465*, 2020. 15
- [30] Hyeonseob Nam, HyunJae Lee, Jongchan Park, Wonjun Yoon, and Donggeun Yoo. Reducing domain gap by reducing style bias. In *Proceedings of the IEEE/CVF Conference on Computer Vision and Pattern Recognition (CVPR)*, pages 8690–8699, June 2021. 3
- [31] Oren Nuriel, Sagie Benaim, and Lior Wolf. Permuted adain: Reducing the bias towards global statistics in image classification. In *Proceedings of the IEEE/CVF Conference on Computer Vision and Pattern Recognition*, pages 9482–9491, 2021. 3, 6, 15, 16
- [32] Taesung Park, Alexei A. Efros, Richard Zhang, and Jun-Yan Zhu. Contrastive learning for unpaired image-to-image translation. In *European Conference on Computer Vision*, 2020. 2, 6, 11, 16
- [33] Taesung Park, Jun-Yan Zhu, Oliver Wang, Jingwan Lu, Eli Shechtman, Alexei Efros, and Richard Zhang. Swapping autoencoder for deep image manipulation. In *Advances in Neural Information Processing Systems*, volume 33, pages 7198–7211, 2020. 4
- [34] Adam Paszke, Sam Gross, Francisco Massa, Adam Lerer, James Bradbury, Gregory Chanan, Trevor Killeen, Zeming Lin, Natalia Gimelshein, Luca Antiga, et al. Pytorch: An imperative style, high-performance deep learning library. *Advances in neural information processing systems*, 32:8026–8037, 2019. 16
- [35] Xingchao Peng, Qinxun Bai, Xide Xia, Zijun Huang, Kate Saenko, and Bo Wang. Moment matching for multi-source domain adaptation. In *Proceedings of the IEEE/CVF International Conference on Computer Vision*, pages 1406–1415, 2019. 3
- [36] Karen Simonyan and Andrew Zisserman. Very deep convolutional networks for large-scale image recognition. In *International Conference on Learning Representations*, 2014. 2, 3
- [37] Amber L Simpson, Michela Antonelli, Spyridon Bakas, Michel Bilello, Keyvan Farahani, Bram Van Ginneken, Annette Kopp-Schneider, Bennett A Landman, Geert Litjens, Bjoern Menze, et al. A large annotated medical image dataset for the development and evaluation of segmentation algorithms. *arXiv preprint arXiv:1902.09063*, 2019. 15
- [38] Eric Tzeng, Judy Hoffman, Trevor Darrell, and Kate Saenko. Simultaneous deep transfer across domains and tasks. In *Proceedings of the IEEE International Conference on Computer Vision (ICCV)*, December 2015. 2
- [39] Hemanth Venkateswara, Jose Eusebio, Shayok Chakraborty, and Sethuraman Panchanathan. Deep hashing network for unsupervised domain adaptation. In *Proceedings of the IEEE conference on computer vision and pattern recognition*, pages 5018–5027, 2017. 3
- [40] Haohan Wang, Zexue He, Zachary L. Lipton, and Eric P. Xing. Learning robust representations by projecting superficial statistics out. In *International Conference on Learning Representations*, 2019. 3
- [41] Tianlu Wang, Jieyu Zhao, Mark Yatskar, Kai-Wei Chang, and Vicente Ordonez. Balanced datasets are not enough: Estimating and mitigating gender bias in deep image representations. In *Proceedings of the IEEE/CVF International Conference on Computer Vision (ICCV)*, October 2019. 1, 2, 6, 16
- [42] Brian Hu Zhang, Blake Lemoine, and Margaret Mitchell. Mitigating unwanted biases with adversarial learning. In *Proceedings of the 2018 AAAI/ACM Conference on AI, Ethics, and Society*, pages 335–340, 2018. 2, 6, 16
- [43] Hang Zhang, Chongruo Wu, Zhongyue Zhang, Yi Zhu, Zhi Zhang, Haibin Lin, Yue Sun, Tong He, Jonas Muller, R. Manmatha, Mu Li, and Alexander Smola. Resnest: Split-attention networks. *arXiv preprint arXiv:2004.08955*, 2020. 15
- [44] Chuanxia Zheng, Tat-Jen Cham, and Jianfei Cai. The spatially-correlative loss for various image translation tasks. In *Proceedings of the IEEE/CVF Conference on Computer Vision and Pattern Recognition (CVPR)*, pages 16407–16417, June 2021. 2
- [45] Kaiyang Zhou, Ziwei Liu, Yu Qiao, Tao Xiang, and Chen Change Loy. Domain generalization: A survey. *arXiv preprint arXiv:2103.02503*, 2021. 3
- [46] Kaiyang Zhou, Yongxin Yang, Yu Qiao, and Tao Xiang. Domain generalization with mixstyle. In *International Conference on Learning Representations*, 2021. 3, 6, 15, 16
- [47] Jun-Yan Zhu, Taesung Park, Phillip Isola, and Alexei A Efros. Unpaired image-to-image translation using cycle-consistent adversarial networks. In *Proceedings of the IEEE international conference on computer vision*, pages 2223–2232, 2017. 2, 6, 11, 16

Data Generation using Texture Co-occurrence and Spatial Self-Similarity for Debiasing Supplementary Material

S.1. Additional Qualitative Results

We show additional results on three datasets. We compare our method with the baseline generative methods: CycleGAN [47], UNIT [27], MUNIT [14], DRIT++ [22], and CUT [32]. Figures S.1, S.2, and S.3 show images generated by pairs of images in each of two rows. Since our proposed method creates an image using the contents and texture information of the pair image, only the texture is transformed like the target image while maintaining the contents of the source image. On the other hand since other methods transform an image in one domain into textures of other domain images, the image is transformed by considering various texture characteristics of the different domain, and thus texture conversion between image pairs cannot be performed.



Figure S.1. Qualitative results of Five vs. Six dataset on five generative models and ours.

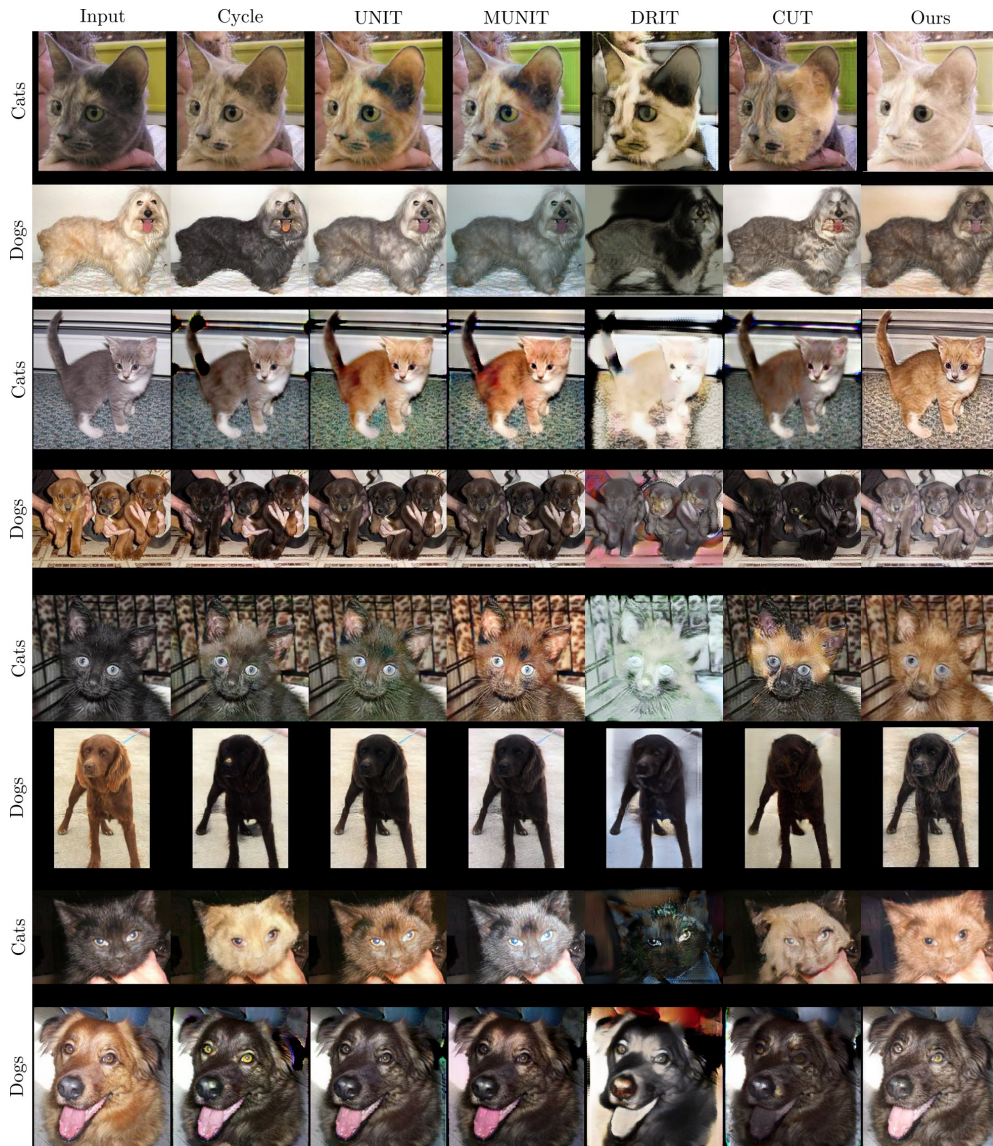


Figure S.2. Qualitative results of Dogs vs. Cats dataset on five generative models and ours.

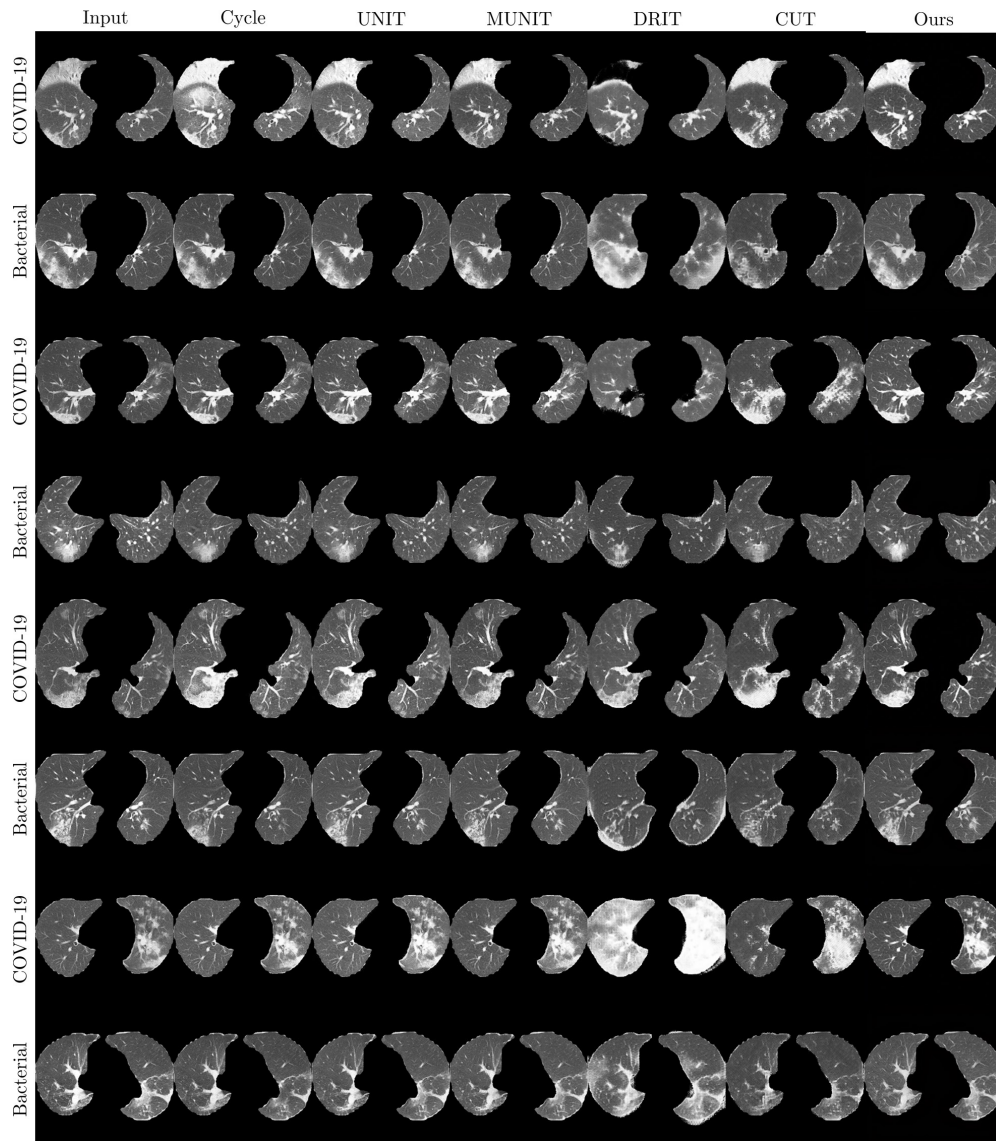


Figure S.3. Qualitative results of COVID-19 vs. Bacterial pneumonia dataset on five generative models and ours.

S.2. Additional Qualitative Results on Multi-class Biased Datasets

We show additional results on multi-class biased datasets. Figures S.4 and S.5 show generated images of our proposed method.



Figure S.4. Qualitative results of Digit dataset on our method.

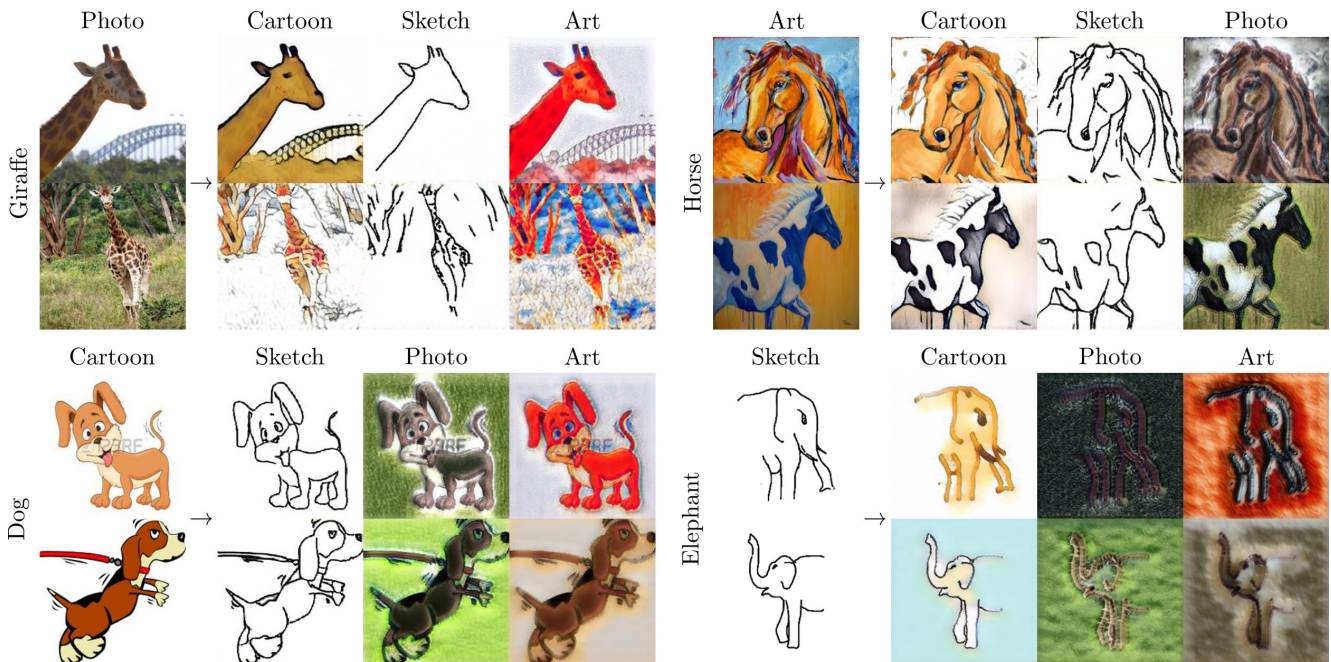


Figure S.5. Qualitative results of Biased PACS dataset on our method.

S.3. Additional Dataset Details

The bias information and dataset statistics of Five vs. Six, Dogs vs. Cats, and COVID-19 vs. Bacterial pneumonia datasets are shown in Table S.1. The bias information and dataset statistics of Digit and Biased PACS datasets are shown in Table S.2. For COVID-19 vs. Bacterial pneumonia dataset, the CT scans were collected at an anonymous medical center from multiple scanners (e.g. Siemens SOMATOM Definition AS+). Window width normalization was applied between 1500 and -600 HU, and the lesions were extracted by applying a Mask-cascade-RCNN-ResNeSt-200 [43] with deformable convolution neural network (DCN) [5] trained on [1, 17, 29, 37].

S.4. Additional Experiment Details

The classifier was trained for 100 epochs with batch size 64, and the learning rate was 0.01. Image size was 224×224 for Dogs vs. Cats, COVID-19 vs. Bacterial pneumonia, Biased PACS, and Inverse Biased PACS datasets, and 32×32 for Five vs. Six and Digit datasets. We performed data augmentation by applying random-affine translation (rotation, translation, and scale), horizontal flips, and color augmentations (i.e., brightness, contrast, saturation, and hue). For domain generalization models, the best hyper-parameters reported in their paper were used for training (e.g., alpha in [46] and probability in [31]), other settings were left the same as the baseline classifier. For generative models, all experiments were trained for 200 epochs approximately and batch size was set to 8, however, UNIT and MUNIT were set to 4 because of hardware (CUDA 9) compatibility. In the classification step, we applied random affine translation (rotation, translation, and scale) and horizontal flips to Dogs vs. Cats, COVID-19 vs. Bacterial pneumonia, Biased PACS, and Inverse Biased PACS datasets, but no augmentation was applied to Five vs. Six and Digit datasets. The rest of settings followed the same as the baseline classifier.

Table S.1. The bias information and statistics of the train/validation/test of Five vs. Six, Dogs vs. Cats, and COVID-19 vs. Bacterial pneumonia datasets. For COVID-19 vs. Bacterial pneumonia, the number of slices and patients are listed.

Split	Five vs. Six		Dogs vs. Cats		COVID-19 vs. Bact.	
	Five	Six	Dogs	Cats	COVID-19	Bacterial
Train	MNIST-M (4,798)	MNIST (5,327)	Bright (4,770)	Dark (4,274)	Non-Cont. (2,119 (46))	Cont. (2,766 (61))
Val	MNIST-M (533)	MNIST (591)	Bright (529)	Dark (474)	Non-Cont. (206 (5))	Cont. (268 (6))
Test	MNIST (5,421)	MNIST-M (5,812)	Dark (3,652)	Bright (3,086)	Cont. (482 (8))	Non-Cont. (326 (8))

Table S.2. The bias information and statistics of the train/validation/test of Digit and Biased PACS datasets.

Split	Five vs. Six		Biased PACS			
	One ~ Four	Five ~ Nine	Dog	Elephant	Giraffe	Horse
Train	MNIST-M (27,085)	MNIST (26,466)	Cartoon (351)	Sketch (666)	Photo (164)	Art (181)
Val	MNIST-M (3,007)	MNIST (2,938)	Cartoon (38)	Sketch (74)	Photo (18)	Art (20)
Test	MNIST (30,596)	MNIST-M (28,909)	Sketch (772)	Photo (202)	Art (285)	Cartoon (324)
			Photo (189)	Art (255)	Cartoon (346)	Sketch (816)
			Art (379)	Cartoon (457)	Sketch (753)	Photo (199)

S.5. Additional Implementation Details

For baseline [12], we employed the official Pytorch [34] ImageNet code¹ for training. To run the experiments in same settings, we integrated all non-generative debiasing implementations to the baseline code. To integrate non-generative debiasing models, we prioritized using the author’s implementation. In case when the author’s implementation is not available, we employed a publicly available code as an alternative. For Learning-to-pivot [28], we used a publicly available code². For Adv debias [42], we used a publicly available code³. For BlindEye [2], we used the author’s implementation of confusion loss⁴. For Learning-not-to-learn [19], we used the author’s implementation⁵. For Not Enough [41], we used the author’s implementation⁶. For domain generalization methods, all author’s implementations are available. For Permuted AdaIN [31], we used the author’s implementation⁷. For MixStyle [46], we used the author’s implementation⁸. To train generative models, all author’s implementations are available. For CycleGAN [47] we used the author’s implementation⁹. For UNIT [27] and MUNIT [14], we used the author’s implementation¹⁰. For DRIT++ [22], we used the author’s implementation¹¹. For CUT [32], we used the author’s implementation¹².

¹<https://github.com/pytorch/examples/blob/master/imagenet/main.py>

²<https://github.com/equalgo/fairness-in-ml>

³<https://github.com/Trusted-AI/AIF360>

⁴https://github.com/mahfujau/domain_adaptation_iccv15

⁵<https://github.com/feidfoe/learning-not-to-learn>

⁶<https://github.com/uvavision/Balanced-Datasets-Are-Not-Enough>

⁷<https://github.com/onuriel/PermutedAdaIN>

⁸<https://github.com/KaiyangZhou/mixstyle-release>

⁹<https://github.com/junyanz/pytorch-CycleGAN-and-pix2pix>

¹⁰<https://github.com/NVlabs/MUNIT>

¹¹<https://github.com/HsinYingLee/DRIT>

¹²<https://github.com/taesungp/contrastive-unpaired-translation>